CORONAL DIAGNOSTIC SPECTROMETER
SoHO

CDS SOFTWARE NOTE No. 54

Version 1 26 May 1999

CDS-GIS Instrument Guide

R.D.Bentley
Mullard Space Science Laboratory
University College London
Holmbury St. Mary
Dorking, Surrey RH5 6NT, UK.

rdb@mssl.ucl.ac.uk

Contents

1 Introduction

The SoHO Coronal Diagnostic Spectrometer (CDS) (Harrison et al., 1995) is designed to measure plasma characteristics with spatial, temporal and spectral resolutions and ranges appropriate to study the structure and evolution of the solar atmosphere. It determines this information through the study of emission line characteristics in the extreme ultra-violet (EUV). The performance requirements of the CDS include the need to observe emission lines between 150 and 800 Å, so as to cover ions formed between 10^4 and a few $\times 10^6$ K. This, and the other scientific requirements of CDS, cannot be achieved by a single instrument. Consequently, the CDS is a double spectrometer having the wide wavelength range of a grazing incidence device plus the stigmatic imaging performance of a normal incidence instrument.

The CDS uses a grazing incidence Wolter type II telescope to simultaneously feed a normal incidence spectrometer (NIS) and a grazing incidence spectrometer (GIS) through a common slit. This document describes the performance of the GIS, and how data from the GIS can be analysed.

The GIS instrument comprises a spherical grating set at grazing incidence, with four micro-channel plate detector systems placed around a Rowland circle. Since the resulting GIS spectra are astigmatic, the instrument builds up images by forming a raster through incremental movements of a pin-hole slit and scan mirror. The field of view of the instrument is 4×4 arcminutes.

The prime goal of the CDS is the measurement of line intensities, not line shapes and shifts. However, it was anticipated that information on modest to high speed flows could be determined.

2 The GIS detector system

Because of the astigmatic nature of the GIS, its detectors only require a one dimension (1-D) capability. The four GIS detector systems are identical, each consisting of a micro-channel plate (MCP) stack in front of a Spiral Anode (SPAN) positional readout (Lapington et al., 1992; Breeveld and Thomas, 1992; Breeveld, 1996). The Z-stack of three MCPs act as a photo-multiplier with each EUV photon producing $\sim 4 \times 10^7$ electrons – the number of electrons produced by an event (the gain) is a function of the bias voltage across the MCP stack. The SPAN readout is illuminated by the electron cloud and accurately determines its position.

The SPAN readout was developed to provide optimal position resolution at a time when space-qualified, fast Analogue to Digital Converters (ADCs) had a maximum resolution of 8-bits. The readout anode consists of a $63 \times 30 \times 3$ mm piece of fused silica which is coated with a 2–3 μm layer of aluminium; a pattern is formed on this using an infra-red laser to create insulating gaps between the electrodes (see figure 1). The anode is divided into a number of identical pitches which are parallel to the dispersion axis of the spectrometer. Each pitch contains the elements of three electrodes (x, y and z) whose areas have the form of damped sine waves – at any position along the anode, the ratio of the fractional charge collected on each electrode is unique. The design of the readout is tuned to the spatial distribution of the electron cloud that emerges from the MCP. The width of the pitch is small with respect to the width of the charge cloud distribution, ensuring that the measured charge is not dependent on the event position in the direction perpendicular to the pitches.

The charge collected on each electrode (Qx, Qy and Qz) is measured using a sample and hold circuit and the values are converted to a digital outputs with 8-bit ADCs (figure 2). The total charge on the three electrodes (Qt = Qx+Qy+Qz) is used as a reference input to the ADC

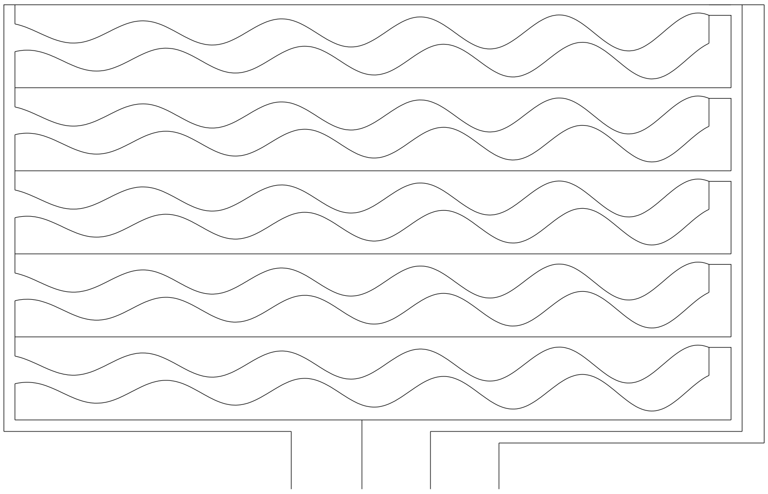

Figure 1: The form of the SPAN readout pattern

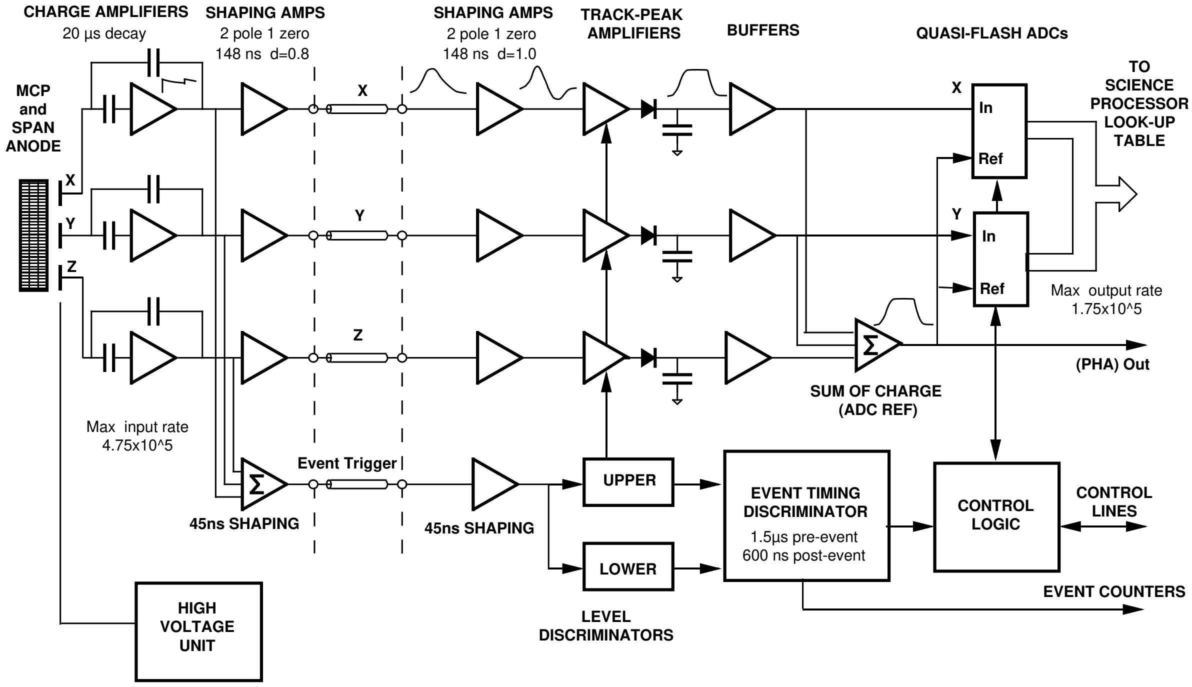

Figure 2: The GIS detector system processing electronics

to normalize the different sized electron clouds. The x and y outputs of the ADCs therefore have the values x=Qx/Qt and y=Qy/Qt. These are used as coordinates in a look-up table (LUT) to determine the actual position of the incoming photon.

The look-up table is assembled by the instrument using an algorithm that calculates the table entries from parameters uplinked from the ground in a GIS setup block (or GSET). The GSET parameters are adjusted for each type of observation, high voltage setting and slit size. They are determined by examining GIS RAW dumps which contain the x and y positions of each photon as output by the ADCs, i.e. the un-encoded look-up values.

The GIS detector system is susceptible to a number of instrumental effects. Some of these

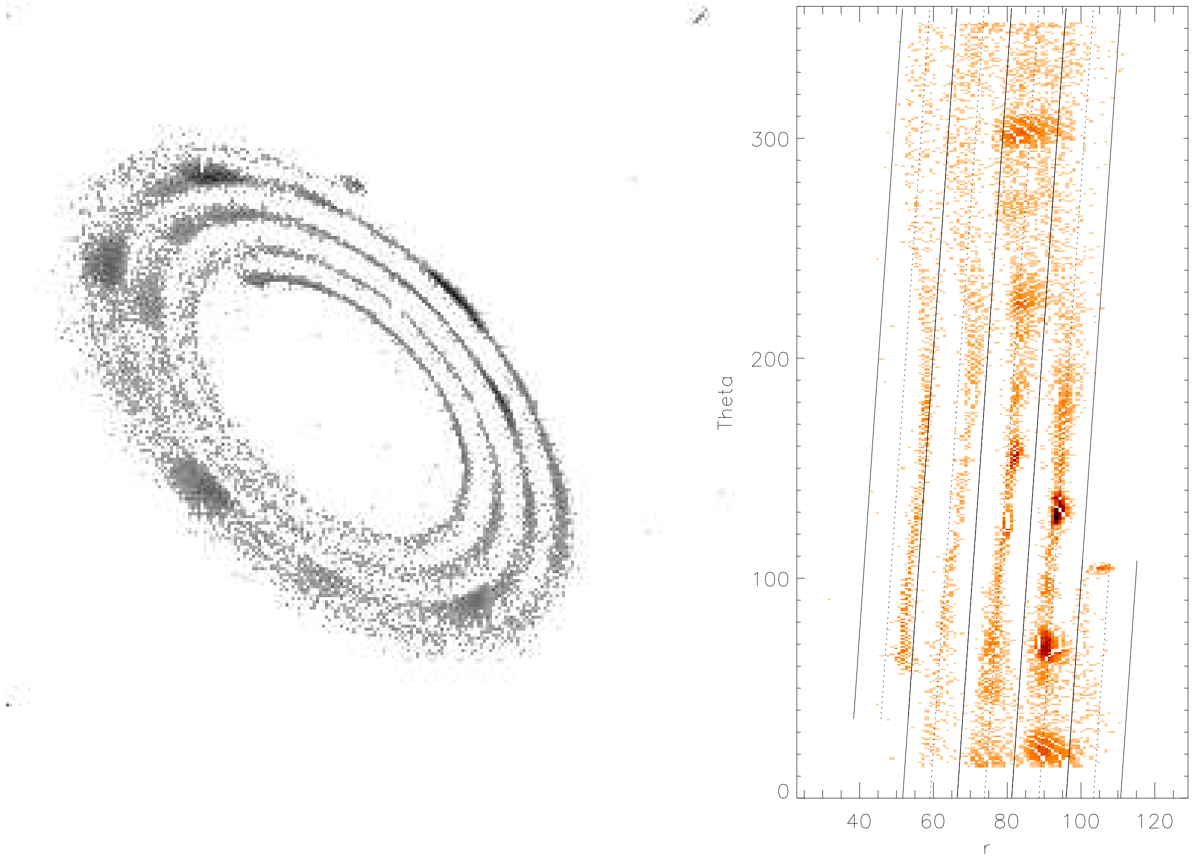

Figure 3: The ADC outputs x and y plotted in a) Cartesian coordinates (top-left) and b) r-theta coordinates (top-right). Each cycle of the sine wave in the SPAN readout pattern is represented by a turn in the spiral in (a) or an arm in (b). The innermost end of the spiral in (a) is equivalent to the bottom of the leftmost strip in (b).

are easier to understand if the GIS RAW dumps are plotted in different ways. The SPAN electrodes take the form of phased, decaying sine waves. When the digitized x and y values output by the ADCs are plotted in Cartesian coordinates they form a spiral (see figure 3a) – the position along the detector is determined by the distance along the spiral. When they are plotted in r-theta space, the values form a series of diagonal stripes, one for each cycle of the sine wave of the SPAN readout (see figure 3b) – here, "r" is the distance from the centre of the spiral, and "theta" the angle around the spiral.

The GSET is adjusted to try to provide the best fit to the stripes on the r-theta plot. Inadequacies in the fit caused by distortions in the spiral, combined with errors in the values of x and y (probably caused by offsets in the analogue electronics), mean that some events are incorrectly encoded to the adjacent arm of the spiral (see Ghosting). The discrete nature of the entries in the look-up table, which try to represent the continuously varying function of the spiral, leads to a digitization noise (see Fixed Patterning).

3 Analysing GIS Data

This section outlines issues relating to instrument calibration and instrument effects that must be considered when analysing GIS data. Further details about these effects, and relevant software, can be found in the User Guide.

3.1 GIS Wavelength Calibration

The wavelength calibration of the GIS was determined by pre-launch calibrations (Bromage et al., 1996; Lang et al., 1999), and has been confirmed in flight. The calibration is automatically applied to GIS spectra as the data are read from a FITS file into a quick-look data structure (QLDS) using **readcdsfits**.

In the GIS system, both the grating and detectors are at a grazing angle to the incident photons of about 70deg. The grating is spherical and the detectors are placed along the Rowland circle. The wavelength calibration across individual detectors can be described as a combination of three functions: a slow quadratic term introduced by the electronic encoding; a complex (almost linear) term from the dispersion from the grating; and a cyclic term because the detectors are flat, not curved with the Rowland circle. This latter function is a third order term and is not normally considered.

As described earlier, the electronic position encoding uses a look-up table (LUT) to determine the event position from the charge measured on the anode electrodes. Two parameters in the GSET used to construct the LUT affect the shape of the wavelength dispersion for the detector; the parameters do not affect the wavelength coverage of the channel.

These (optical and electronic) effects are folded into the wavelength calibrations that have been prepared for each GSET. Minor residual variations (up to 20% of a line width) are expected between observations – these are left to the user to accommodate within their software.

3.2 GIS Intensity Calibration

The GIS intensity calibration was determined before launch in tests at RAL (Bromage, et al., 1996; Lang et al., 1999). The intensity calibration has been confirmed using a differential emission measure (DEM) analysis of in-flight data (Landi et al., 1998). In addition, a number of cross-calibration observations have been made in collaboration with the SUMER instrument on SoHO, flights of the SERTS rocket in 1996 and 1997, and the Wood/Hassler rocket in 1997 – these data are still being reduced in preparation for an inter-instrument calibration meeting.

Before the intensity calibration can be applied to GIS data, a number of corrections must be made to the data. This is done by the analysis routine **gis_calib** (see the User Guide).

3.2.1 Corrections for Electronics dead-time

In common with most detector systems of this type, there are dead-times associated with the processing electronics. The required corrections are discussed in the GIS User Guide. They affect the data at relatively high countrates and only limit the GIS throughput above 10^5 counts per second:

i) An extending dead-time for each detector related to the time taken for analogue electronics to process an event and settle to their nominal level.

ii) A non-extending dead-time, affecting all detectors, related to the multiplexing of the position data produced by the four detector systems into one stream. This is sometimes called quiz-show dead-time.

iii) A non-extending dead-time, affecting all detectors, related to the FIFO buffer. This buffer evens out the flow of data into the CDS CDHS unit.

3.2.2 Corrections for Localized Sensitivity Changes

It is common to express the sensitivity of an instrument in terms of an overall sensitivity (or effective area), and as a map of relative sensitivity across the readout window. The GIS detector systems show very little variation across their 2048 pixels, except at the very ends (see Edge Effects), and in the region of very intense lines. Localized high count-rates affect the micro-channel plate and and must be taken into account. These are outlined below and discussed in detail in Breeveld (1996).

i) **Count-rate gain depression (CRGD)**: A micro-channel plate (MCP) works by creating an avalanche of electrons when a photon enters a channel in the MCP. There is a finite time (between 3 and 100 ms) required to recharge the channels after a pulse of electrons has been released and the gain that can be sustained by the channel plate is inevitably reduced as the photon countrate increases. The countrate per pore is the most important parameter – a high countrate across the whole plate does not induce gain depression (although electronic deadtimes may affect the overall throughput). In the GIS detectors, this type of count-rate gain depression (CRGD) is observed in the regions of intense spectral lines. The effect can be corrected up to a predetermined countrate in a pixel – beyond that the region of the detector is marked as uncalibrated.

ii) **Long-term gain depression (LTGD)**: In regions close to excessively bright lines in the GIS (e.g. He II at 304 Å), long term depressions in the gain of the MCP are observed. The exact cause of this is not known, but it is assumed to result from a reduced efficiency in the production of secondary electrons from the channel walls, possibly due to the creation of electron traps within the lattice of the MCP material. The degradation depends on the total charge extracted, not the rate of extraction or gain.

The overall gain of the GIS detector system is maintained by adjusting the detector high voltage settings. The detectors are usually run so that the pulse height distribution is fully saturated (the FWHM of the distribution being between 80 and 120%). While the high voltage can be adjusted to correct the depressed gain in the regions affected by LTGD, such adjustments adversely affect the gain in other parts of the detector. Because of difficulties in monitoring the degree of the LTGD, it has proved impossible to accurately correct the gain depression in the region of the brightest lines. As a consequence, regions close to such intense lines are marked as uncalibrated.

3.2.3 Other corrections

The GIS detector system suffers from ghosting, or the incorrect determination of event position in the detector. The correction for ghosting involves moving counts from one part of the detector to another and this must be done before the intensity calibration is applied. Ghosts are discussed further below, and in the User Guide.

3.3 GIS Instrumental Effects

3.3.1 Fixed patterning

Position encoding of the GIS detector is implemented using a look-up table (LUT) – the coordinates used to determine the converted position from the LUT are provided by the digitized charge from the x and y electrodes. An inadequate resolution in the LUT has resulted in fixed patterning, where adjacent pixels share varying amounts of the incoming counts (Breeveld et

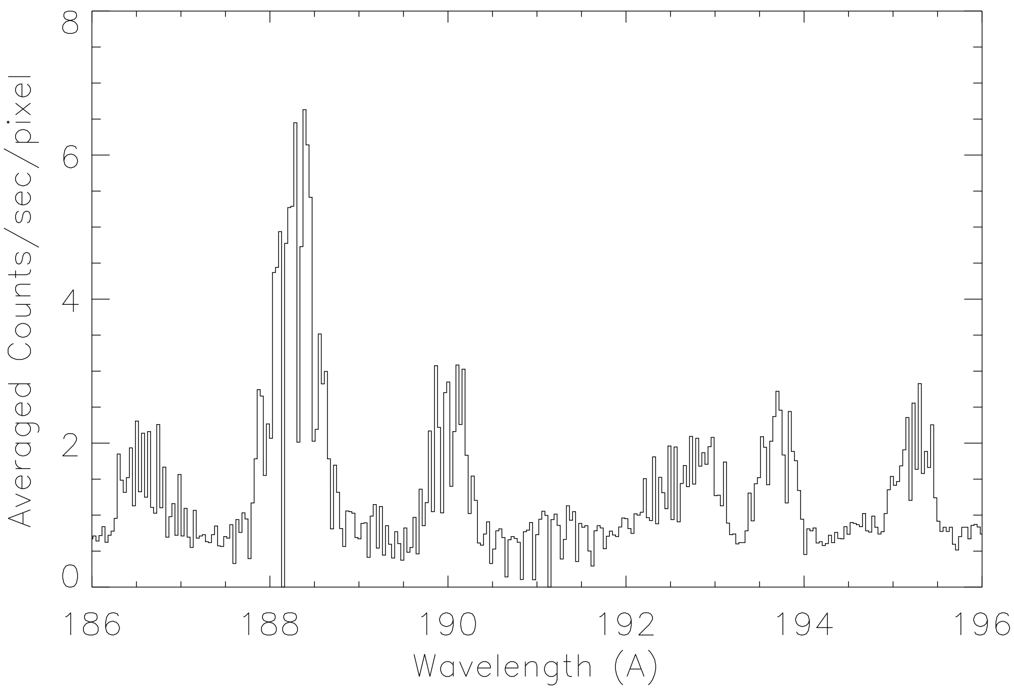

Figure 4: An example of the fixed patterning seen in the GIS.

al., 1992). Although the positions of the photons are shifted, the total number of counts is conserved and line intensities are unaffected.

The affects of fixed patterning can be seen in figure 4. Data points drop to near zero, while adjacent points are enhanced in intensity. Fixed patterning is also visible on the r-theta plot in figure 3 as a “wood-grain” pattern superimposed on the spiral arms.

Before the GIS data are analysed, a simple smoothing algorithm is applied to “reduce” the fixed patterning.

3.3.2 Line widths and profiles

The GIS line widths are larger than expected and their shapes are anomalous. The line profiles cannot be fitted with single Gaussians – their unusual nature was reported by Bromage et al. (1996) in their analysis of data from ground calibrations. Typical widths for lines observed by the GIS with different slits are shown in figure 5 - this also shows the expected line widths (from the “Blue Book”), and the “stim pulse” line widths. It is unclear whether the cause of the anomalous profiles is an optical or detector effect.

The detector processing electronics can be tested using stim pulses that are applied to pads on the back face of the anode plate, and capacitively couple to the anode electrodes. The stims are normally switched off, but can be commanded ON from the ground. That the stim pulses form a narrow profile implies that the anomalous width of the spectral lines is not caused by the processing electronics but must arise before the SPAN readout system. This implies an effect either related to the MCP, or within the optics of the spectrometer.

The anomalous line shapes prohibit a detailed study of the plasma dynamics. However,

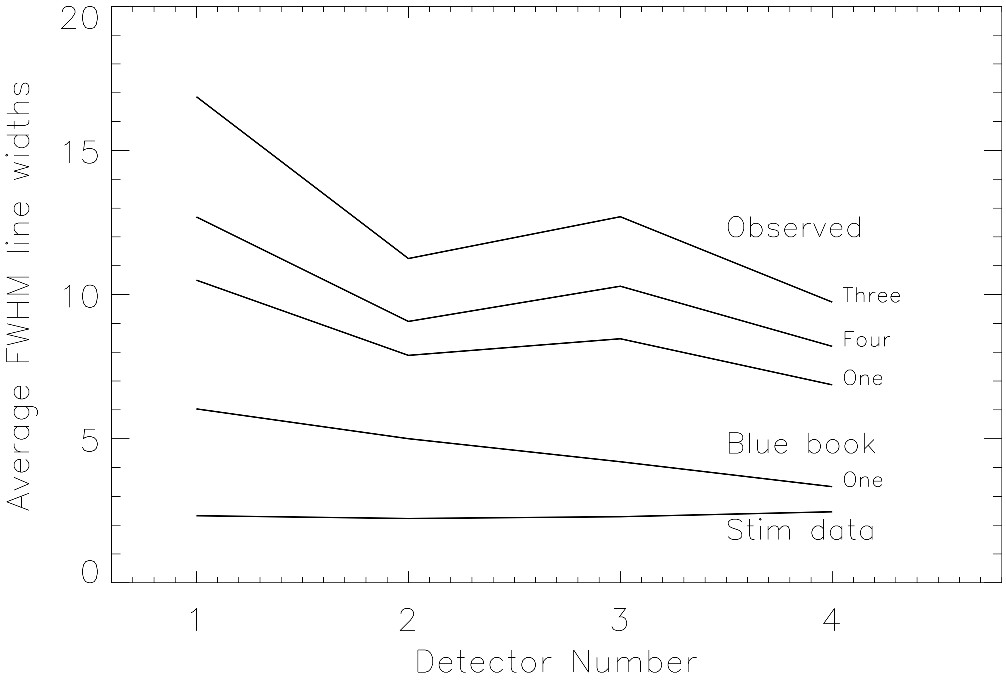

Figure 5: A comparison of line widths of the GIS (in pixels). The bottom line is the width of the stim; the next line is the expected "Blue Book" width for slit one, and the top three curves the observed widths for slits one (2×2 arcsec), three (8×50 arcsec), and four (2×240 arcsec),

since the counts are just redistributed in the vicinity of the line and not lost, the primary objective of the GIS system – to measure line intensities – is not affected.

The NIS line widths are also slightly larger than expected and it has been suggested that some of the difference in both instruments might be due to the fact that the pre-flight measurements were made using a narrow-beam source.

3.3.3 Edge Effects

At the ends of the GIS detectors, particularly the long wavelength end, the background level is seen to increase. This is partly due to a compression in the wavelength scale in the end regions of the detector where it deviates from the assumed parabolic shape. Other possible causes include some form of secondary emission from the spectrometer structure.

In the GIS-3 and GIS-4 channels, an edge effect that is due to real He continuum is visible. This is seen only in observations made on the solar disk, but has not been fully quantified. In the case of GIS-2, there are very strong lines at the beginning of detector which should not be confused with edge effects.

At the moment, no correction is made for edge effects.

3.3.4 Ghosting

The performance of the spiral anode readout used for the GIS detectors can be affected by an ambiguity in the position of incoming photons. This occurs at certain phases of the sine

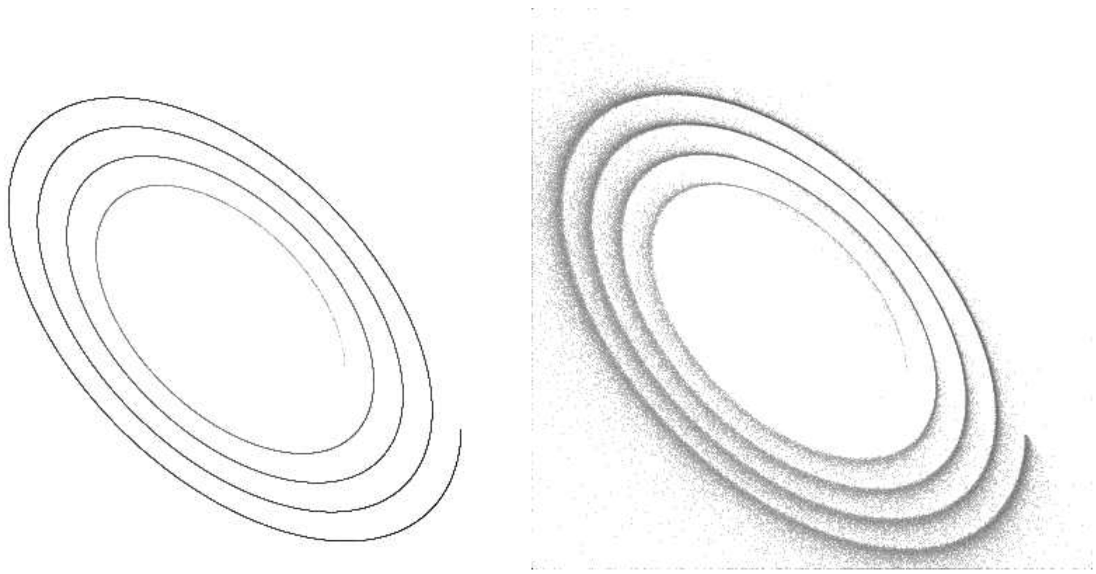

Figure 6: This plot shows a simulation of ghosting: an ideal, synthetic spiral (left), and its appearance when offsets are introduced into the analogue electronics (right). Compare the right-hand image with the spiral in figure 7. In the simulation, the ratio of the offsets for x,y and z was 2:2:1.

wave pattern of the SPAN readout and translates into "ghost" in some regions of the resulting spectrum. The counts in the ghosts must be added to the original lines before an intensity calibration can be performed.

The performance requirements specified for the GIS included the ability to handle a high count rate – up to 20,000 counts per second per detector. The analogue to digital converters and other analogue components were selected to meet this requirement within the power constraints of the instrument. However, when the flight model instrument was integrated, the processing electronics were found to be affected by electronic noise. One consequence is the appearance of small offsets in the analogue electronics that produce increased errors in the x and y outputs of the analogue to digital converters – this translates into a positional uncertainty when the event pulse heights are small. The effect has been simulated and the results of the model agree well with the observed spiral (see figure 6) – ghosts occur where the width of the spiral is broadened by the effects of the offsets. The spiral arms overlap each other in these regions of the detector and this introduces a leaking of position data in the resulting spectrum.

This can also be seen in the three plots in figure 7 which were generated from an observation of the quiet Sun. In this figure the darker regions in the spiral are the spectral lines; when plotted in r-theta space, some of these are seen to spread, or ghost into adjacent arms of the spiral. The lower plot shows the spiral unravelled and then summed to produce a spectrum. Ghosts can be seen as features entering from the top or bottom of the greyscale strip where they have spread from an adjacent arm of the spiral; the direction of entry depends on whether the line has ghosted from the blue or red side.

It can be seen that the ambiguity (or ghosting) in spectral data does not occur over the whole spectral range, and that where ghosting occurs it is confined to specific locations in adjacent spiral arms. This allows the GIS analysis software (**ghost_buster** and associated routines) to characterize the ghosts as detailed in the **User Guide**.

When correcting for ghosts, the counts in the ghosts must be added to the counts at the original location to produce the observed line intensity which can then be corrected for instrumental effects and calibrated. The best way to proceed from this point is still being investigated. One way is to perform a fit to the data after the ghosted counts have been moved back to their orig-

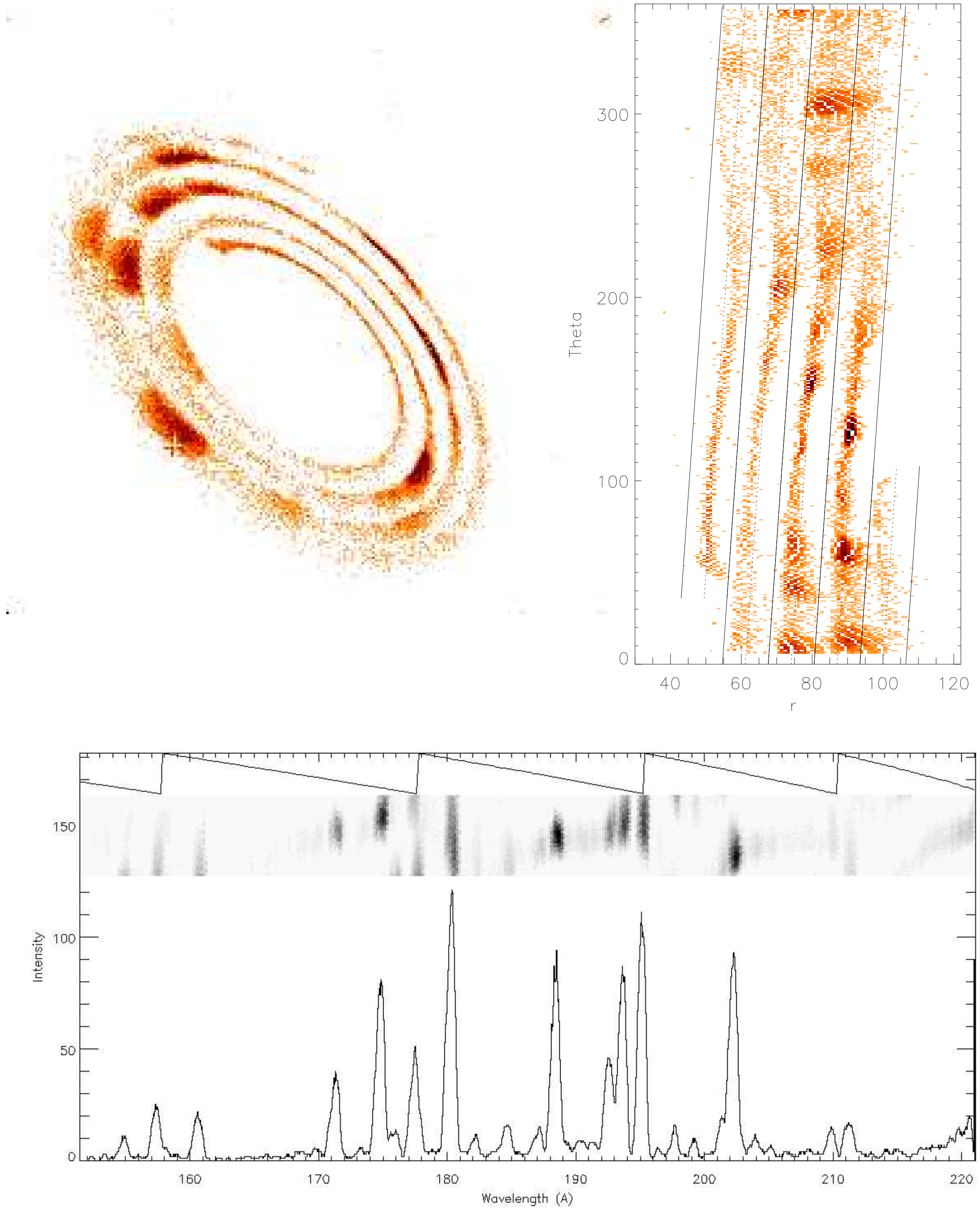

Figure 7: A GIS RAW dump plotted in three different ways: a) in Cartesian coordinates (top-left), b) in r-theta coordinates (top-right), and c) as a strip that follows the spiral (bottom) – a vertical summation of this produces the GIS spectrum. The innermost end of the spiral in (a) is equivalent to the bottom of the leftmost strip in (b) and long wavelength (rightmost) end of the spectrum in (c) – i.e. the wavelength decreases as you move outwards around the spiral. The sawtooth in (c) indicates the theta position along each spiral arm. The ghosts result from a tendency for counts to spread from one arm of the spiral to another; they occur where the phase of the spiral is the same. In plot (c), the ghosts appear as injections of counts from the top or bottom of the intensity map.

inal locations. Alternatively, given a knowledge of the degree of ghosting for each line (which depends on GSET and is indicated in the Ghost Information Files), a ghosted spectrum can be generated and combined with the un-ghosted spectrum in a multi-component spectral fit to the original data; the fitted ghost can then be relocated and the restored spectrum calibrated. Both approaches have drawbacks and the two techniques are being intensively studied.

Acknowledgements Many of the figures in this report have been prepared with the help of Carl Foley, Jon Lapington and Matt Whyndham.

References

[1] Bromage, B.J.I., Breeveld, A.A., Kent, B.J., Pike, C.D., and Harrison, R.A., 1996, "Report on the pre-launch Calibration of CDS", UCLan Report CFA/96/06.

[2] Breeveld, A.A., 1996, "Ultraviolet Detectors for Solar Observations on the SOHO Spacecraft", University of London Ph.D. Thesis.

[3] Breeveld, A.A. and Thomas, P.D., 1992, "The Grazing Incidence Detectors for the SOHO Coronal Diagnostic Spectrometer", Proceedings of an ESA Symposium on Photon Detectors for Space Instrumentation, p 237-241.

[4] Breeveld, A.A., Edgar, M.L., Lapington, J.S. and Smith, A., 1992, "The effects of charge cloud size and digitization on the SPAN anode", in "EUV, X-ray, and gamma-ray instrumentation for astronomy III", Proceedings of the Meeting, San Diego, CA, July 22-24, 1992, p. 315-326.

[5] Harrison, R.A. et al., 1995, "The Coronal Diagnostic Spectrometer for the Solar and Heliospheric Observatory", Sol. Phys., 162, 233.

[6] Harrison, R.A., and Fludra, A., 1995, "The Coronal Diagnostic Spectrometer for the Solar and Heliospheric Observatory", the "BLUE book", RAL Report SC-CDS-RAL-SN-95-001.

[7] Landi, E., Del Zanna, G.; Breeveld, E.R.; Landini, M.; Bromage, B.J.I.; Pike, C.D., 1999, "Relative intensity calibration of CDS-GIS detectors on SOHO using a plasma diagnostic technique", Astronomy and Astrophysics Supplement, v.135, p.171-185.

[8] Lang, J., Kent, B.J., Breeveld, A.A., Breeveld, E.R., Bromage, B.J.I., Hollandt, J., Payne, J., Pike, C.D., and Thompson, W.T., 1999, "The Laboratory Calibration of the SOHO Coronal Diagnostic Spectrometer", RAL Report RAL-TR-1999-036.

[9] Lapington, J.S., Breeveld, A.A., Edgar, M.L. and Smith, A., 1992, "Performance characteristics of SPAN position readout systems", in "EUV, X-ray, and gamma-ray instrumentation for astronomy III", Proceedings of the Meeting, San Diego, CA, July 22-24, 1992, p. 303-314.